

Poly(phenylene oxide) and Renewable Polyamide 11 Blends Compatibilized by Ethylene-*n*-Octene Copolymer

Regina Jeziorska*, Agnieszka Abramowicz, Agnieszka Szadkowska, Anna Pasnik and Ewa Spasowka

Department of Polymer Technology and Processing, Industrial Chemistry Research Institute, Rydygiera 8, 01-793 Warsaw, Poland

Received January 23, 2018; Accepted January 24, 2018

ABSTRACT: Poly(phenylene oxide)/renewable polyamide 11 (PPO/PA11 20/80) blends toughened with glycidyl methacrylate grafted ethylene-*n*-octene copolymer (GEOC) were prepared in a co-rotating twin-screw extruder. The reaction between GEOC and PPO/PA11 blend was analyzed by gel content tests. The morphology of PPO/PA11/GEOC blends was observed by scanning electron microscope. The SEM results showed that PPO formed the continuous phase, though it is a minority component of blends. With increasing GEOC content from 5 to 15 wt% the morphology of the blends transformed from droplet-matrix to co-continuous structure, in which both PA11 and PPO phases are continuous. The blend with co-continuous morphology had better mechanical properties than those with droplet-matrix morphology. The impact strength of the PPO/PA11/GEOC blends was much higher compared to the one without GEOC as well as PA11 due to the compatibilizing effect, which was also proved by DSC analysis, rheological behavior (MFR, DMTA) and tensile properties.

KEYWORDS: Compatibilization, elastomer, PPO/PA11 blends, toughening

1 INTRODUCTION

Polymer blends have been widely investigated for several decades since they offer new high-performance polymeric materials. However, most polymer blends are immiscible and their properties strongly depend on the formed morphology and interfacial adhesion of the blend components. Two major kinds of morphologies are possible in the case of melt blended immiscible polymers: the matrix-dispersed structure and the co-continuous structure. However, the co-continuous morphology offers a better combination of the component properties than the dispersed type structure [1–3].

Blends of polyamide 6 (PA6) and poly(phenylene oxide) (PPO) are of interest as high-performance systems [4–7]. However, PPO is an amorphous polymer and PA6 is a crystalline polymer which is thermodynamically immiscible and generally shows deterioration in impact and tensile strength. Blending with suitable elastomeric materials has been considered one of the most effective methods to improve toughness of brittle materials [8]. Toughening of rubber-toughened

polymer strongly depends on the amount, particle size, and properties of elastomers, as well as the interactions between phases determining the mechanical properties of the toughened polymers [9]. There are many ways for PPO/PA blends to be compatibilized, including various maleic anhydride (MA) grafted copolymers [10–12]. MA-grafted PPO has also been reported as a good reactive compatibilizer for PPO/PA6 blends [3,13]. Son and Lee [13] successfully produced reactive compatibilized PPO/PA66/elastomer blends by the one-step method in which maleation of PPO/SEBS and reactive blending of PPO/SEBS/PA66 occur simultaneously in a twin-screw extruder. The mechanical properties of the blends obtained by the one-step method were similar to those obtained by the traditional two-step one. Maleic anhydride grafted polyolefin elastomer poly(ethylene-1-octene) (POE-g-MA) has also been reported as an effective compatibilizer for PPO/PPO-g-MA/PA6 (35/35/30) blend [12]. It was proved that the particle size below 1 μm of POE-g-MA can be controlled in the polymer matrix by the MA graft ratio, which was when the graft ratio is 0.46 wt%, resulting in effective toughening. Lai [14] used PPO-g-PA6 grafted copolymer as the compatibilizer for PPO/PA6 blends, called physical compatibilization. Mostly, polymers or copolymers miscible or

*Corresponding author: regina.jeziorska@ichp.pl

DOI: 10.7569/JRM.2018.634114

compatible with PPO bearing functional groups capable of reacting with PA are used.

Biocompatible polyamide 11 (PA11) is an interesting commercial aliphatic polyamide with great environmental benefits. PA11 shows excellent properties such as good oil resistance. Moreover, it is less hydrophilic than commonly used polyamides (6 and 66) [15]. Therefore, PA11 is widely used as an engineering polymer in a large range of applications from automotive industry to food packaging. Recent results show that PA11 forms a good interface with flax fibers [16,17], which results in specific properties with fiber volume fraction reaching 70% [18]. Moreover, the recycling stability of unidirectional flax fiber reinforced bio-based PA11 (50 vol%) in comparison to PP/PPgMA-flax (49 vol%) has been studied [19]. To the best of our knowledge, PPO and biobased PA11 blends have not yet been studied.

Within this context, rubber-type polyolefin ethylene-*n*-octene copolymer (EOC) grafted with glycidyl methacrylate (GMA) was used as a compatibilizer for poly(phenylene oxide)/polyamide 11 (PPO/PA11) (20/80) blend. It can be expected that GMA grafts of EOC could react with the amine end group of PA11, forming covalent bonds between those two polymers via reactive extrusion according to the scheme presented in Figure 1, resulting in increased viscosity of PA11 and finer dispersion of dispersed phase. The effects of GMA grafted EOC (GEOC) on the morphology, melting and crystallization behaviors, and dynamic mechanical properties of PPO/PA11 (20/80) blend were investigated using scanning electron microscopy (SEM), differential scanning calorimetry (DSC), and dynamic mechanical analysis (DMTA), respectively. Furthermore, impact strength and tensile properties of PPO/PA11/GEOC blends were also studied. Finally, properties of the blend with 15 wt% GEOC were compared to the one with 15 wt% EOC.

2 EXPERIMENTAL

2.1 Materials

Amorphous poly(phenylene oxide) (PPO, Noryl V0150B) was purchased from Sabic GE Plastics Co., USA, with melt flow rate of 4 g/10 min (ISO 1133 at 300 °C and 5 kg). Semicrystalline polyamide 11 from renewable sources (PA11, Rilsan PA11) was supplied by Arkema, France, with melt flow rate of 22 g/10 min (ISO 1133 at 235 °C and 10 kg). Ethylene-*n*-octene copolymer (EOC), Engage 8200, was obtained from DuPont Dow Elastomer Ltd., Wilmington, DE. Its octane content and melt-flow rate were 38 wt% and 5 g/10 min (ISO 1133 at 190 °C and 2.16 kg), respectively. Glycidyl methacrylate (GMA), styrene comonomer and dicumyl peroxide (DCP) were commercial reagents purchased from Aldrich Chemicals.

2.2 Preparation and Characterization of GEOC

Rubber-type polyolefin ethylene-*n*-octene copolymer was grafted with glycidyl methacrylate (GMA) via reactive extrusion to obtain a grafting yield of 0.68 wt% according to the process published elsewhere [20–22], and was used as an impact modifier as well as a compatibilizer for PPO/PA11 blend in concentrations of 5, 10 or 15 wt%. GEOC was prepared as follows: EOC, GMA, styrene comonomer, and DCP were mixed in the internal mixer and, subsequently, the mixture was extruded using a ZE-33×25 twin-screw co-rotating extruder (Berstorff) with a length/diameter ratio (L/D) of 33. The temperature increased from 160 °C at the barrel to 190 °C at the die. The output was 4 kg/h, and the screw speed was 100 rpm. The styrene comonomer was used as a donor of electrons to increase the grafting ratio of GMA onto EOC, while

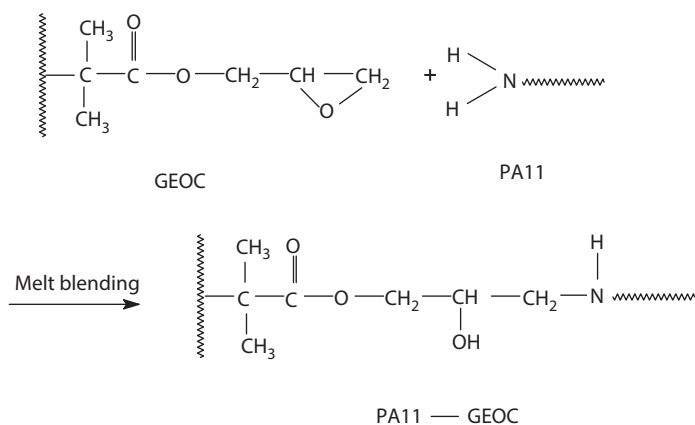


Figure 1 Schematic description of the *in-situ* compatibilization.

eliminating the competitive GMA homopolymerization [21].

The GMA calibration curve based on the absorbance of the integral analytical band from the expressed in % (wt/wt) GMA concentration was determined by the FTIR spectra (PerkinElmer System 2000 spectrometer, samples in a 0.5–3.5 wt% GMA solution in chloroform on KBr pellets of 0.07 mm thickness absorption layer). The absorbance of the analytical band derived from the stretching vibration of the ester carbonyl group with a maximum at 1729 cm^{-1} was measured. The baseline was plotted at the base of the analytical band in the wavelength range 1766–1690 cm^{-1} . The correlation coefficient was 0.9999 [22].

The GMA grafting yield was measured by Fourier transform infrared (FTIR) spectroscopy. FTIR was performed on a PerkinElmer System 2000 spectrometer on films of 0.07 mm thickness. The spectra were obtained by collecting 64 scans between 500 and 4000 cm^{-1} with a resolution of 2 cm^{-1} . The FTIR spectra of samples were recorded after extraction by xylene. The extraction was carried out in boiling xylene for 2 h. The grafted EOC was precipitated with ethanol from a hot solution (xylene/ethanol 1:5 [v/v]) and after filtration was dried at 40 °C for 4 h. The ungrafted GMA remained in the solution. The absorbance of the analytical band was determined and the GMA content was calculated from the calibration curve. The measured grafting yield was 0.68 wt%.

Dynamic viscosity of EOC and GEOC was measured with a Malvern Kinexus Pro rheometer, using the cone of 25 mm diameter as upper geometry and the plate of 55 mm diameter as lower geometry. All measurements were performed at 180 °C.

2.3 Preparation of Blends

Before blending, PPO and PA11 were dried at 85 °C under a vacuum for about 12 h. Blends of PPO/PA11 (20/80) with 5, 10 and 15 wt% of GEOC or 15 wt% EOC were prepared by melt compounding using a semi-industrial twin-screw co-rotating extruder (KraussMaffei Group) with a screw diameter (D) of 25 mm and length to diameter ratio of 51, based on the reported method [23]. Separate gravimetric feeders were used for PPO, PA11 and ethylene-*n*-octene copolymer (GEOC or EOC). The temperature increased from 215 °C at the barrel to 270 °C at the die, and the screw speed was 200 rpm. The extruder was equipped with a highly efficient vacuum vent to remove unreacted species and reaction by-products. After compounding, the material was extruded from the die with two cylindrical nozzles of 4 mm diameter, and then cooled rapidly in the air and pelletized with an adjustable rotating knife into 4 mm pellets.

2.4 Gel Content Tests

The gel content was determined as follows: 250 mg sample was dissolved in 50 ml chloroform at room temperature. The soluble part was removed by filtration until no deposition could be detected in chloroform solution by adding excess acetone. Then the insoluble component was dried and then dissolved in 50 ml nitric acid at room temperature for 4 h. The soluble part was removed by filtration until no deposition could be detected in nitric acid solution by adding excess alcohol. The insoluble gel was washed well with alcohol, dried, and weighted. The percentage of the insoluble gel was defined as the gel content.

2.5 Scanning Electron Microscopy

A JEOL JSM 6100 scanning electron microscope (SEM) was used to study the morphology of PPO/PA11 blends. The samples were etched by chloroform and nitric acid, a good solvent for PPO and PA11, respectively, before measurement. The impact fracture surfaces were coated with gold to avoid electrical charging and to increase image contrast.

2.6 Differential Scanning Calorimetry

Thermal analysis was performed on a Mettler-Toledo (Switzerland) differential scanning calorimeter at a heating rate of 10 °C/min, in nitrogen atmosphere, with a scan range of room temperature to 300 °C. From these scans the melting temperature (T_m), melting enthalpy (ΔH_m), crystallization temperature (T_c) and degree of crystallinity (X_c) were measured. The degree of crystallinity of the samples was calculated from the melting enthalpy results (ΔH_m) of each sample using Equation 1, where w_{PA11} is the mass fraction of PA11 in the samples, ΔH_m is the experimental melting enthalpy and ΔH_m° is the melting enthalpy for 100% crystalline PA11, 189 J/g [24].

$$X_c = \frac{\Delta H_m}{w_{PA11} \Delta H_m^\circ} \cdot 100\% \quad (1)$$

2.7 Mechanical Properties Tests

Tensile and impact bars were molded at 220–245 °C using an Arburg 420 M single-screw injection machine (Allrounder 1000-250, Germany). The mold temperature was kept at 80 °C. Tensile properties were measured with an Instron universal testing machine (model 4505) according to ISO 527 standard test procedure. Tensile strength and elongation at break were determined using a clip-on incremental extensometer

(Instron) at a crosshead speed of 50 mm/min, whereas tensile modulus was measured at the speed of 2 mm/min. Notched Charpy impact tests were performed on $80 \times 10 \times 4$ mm specimens with a V-shaped notch on a Zwick impact tester according to ISO 179 standard. All tests were carried out at room temperature. Five measurements were done for each data point in all mechanical property tests. Prior to testing, the samples were stored at 23 °C and 50% RH for 10 days, according to ISO 527 and ISO 179 standards.

2.8 Rheological Measurements

Melt flow rate (MFR) of the blends was measured at 235 °C and 10 kg load according to ISO 1133 standard. Dynamic mechanical analysis (DMTA) was performed on a Rheometrics RDS 2 dynamic analyzer, using rectangular bars with dimensions of $38 \times 10 \times 2$ mm. The torsion method was used at a frequency of 1 Hz, at strain level of 0.1% in the temperature range of -150 to 200 °C. The heating rate was 3 °C/min.

3 RESULTS AND DISCUSSION

3.1 Characterization of EOC Functionalization and PPO/PA11 Blends Compatibilization

To improve the mechanical performance of PPO/PA11 (20/80) blend, a method for ethylene-*n*-octene copolymer functionalization was developed [21]. Glycidyl methacrylate was melt grafted onto EOC in the presence of a styrene comonomer, which was used as a donor of electrons to increase the grafting yield of GMA onto EOC, while eliminating the competitive GMA homopolymerization [20, 21].

Figure 2 shows the FTIR spectra of GMA, EOC and GEOC. A strong peak can be observed at 1729 cm^{-1} for GEOC. It is characteristic of the C=O stretching vibration of the ester carbonyl group introduced by GMA. A weak peak of the C–O stretching band at 1176 cm^{-1} is also visible. These results indicate the successful grafting reaction of GMA onto EOC chains according to the scheme presented in Figure 3.

The effect of GMA on the melting and crystallization behaviors of EOC was studied using DSC. The values of the crystallization temperature (T_c), melting temperature (T_m) and melting enthalpy (ΔH_m) are presented in Table 1. The analysis of DSC data indicates that melting as well as crystallization behaviors were significantly affected by GMA. Indeed, from Table 1 it can be observed that T_m of GEOC was 61 °C higher but T_c was 4 °C lower compared to EOC. Moreover, EOC showed a single melting peak, while GEOC exhibited

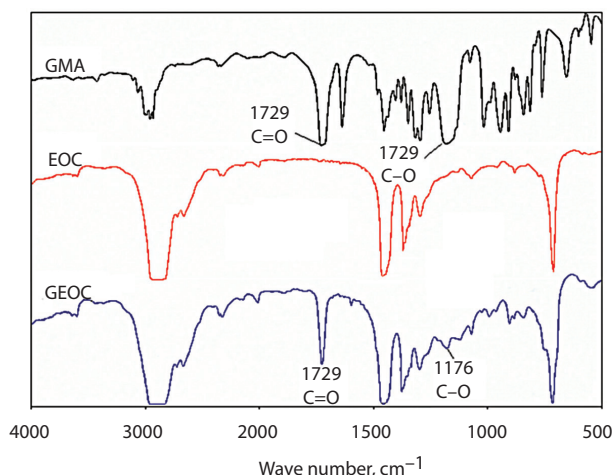


Figure 2 FTIR spectra of GMA, EOC and GEOC.

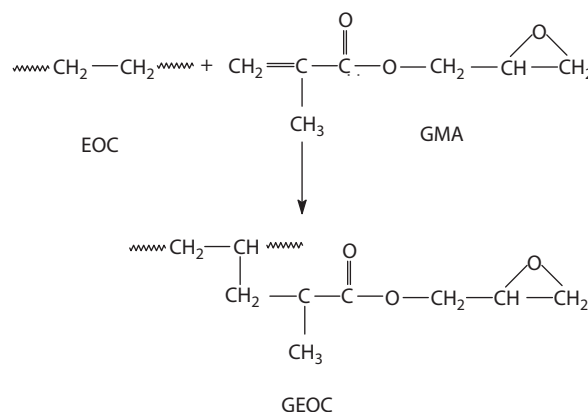


Figure 3 Schematic description of the *in situ* functionalization.

Table 1 Influence of GMA on the thermal properties of EOC.

Sample	T_c (°C)	T_m (°C)	ΔH_m (J/g)
EOC	50	60	36.8
GEOC	46	101; 121*	48.8

*the main effect

double peaks. Simultaneously, melting enthalpy increased by over 30%. These changes might suggest a significant increase in free surface energy in the crystalline phase and better organization of the crystalline phase of GMA grafted EOC [25].

The melt viscosity of GMA grafted EOC was studied using a capillary flow rheometer at 180 °C. The data of GEOC was compared to that of EOC in Figure 4. It was observed that at 180 °C the melt viscosity of GEOC is much higher than EOC. It can be expected that

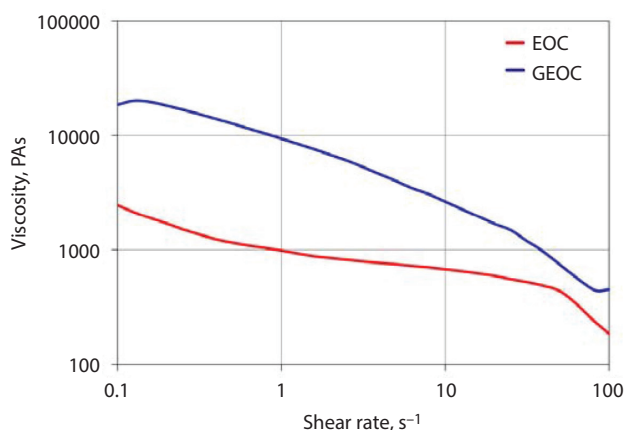


Figure 4 Viscosity versus shear rate for EOC and GEOC at 180 °C.

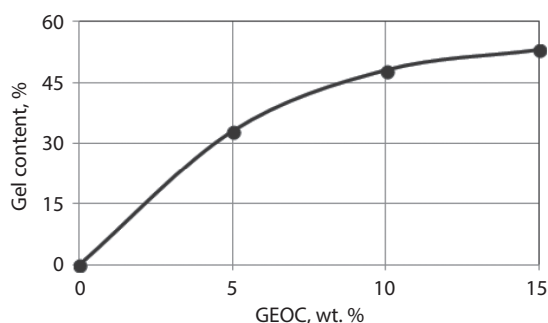


Figure 5 Effect of GEOC on the gel content of PPO/PA11/GEOC blends.

the melt viscosity of PA11 will increase when GEOC is introduced into the PPO/PA11 blend. Moreover, when the viscosity of PA11 meets that of PPO the co-continuous morphology of PPO/PA11 blends can be obtained, which is a key factor to improve toughness of blends [1].

The scheme presented in Figure 1 briefly presents the process of the *in-situ* compatibilization conducted for PPO/PA11 blend, where part of GEOC formed graft copolymer with PA11 *in situ*, which can efficiently control the phase morphology of the blends during compounding. The amount of GEOC–PA11 formed *in situ* was calculated by the gel content tests. The blend sample was successively extracted by chloroform and then by nitric acid. The residue insoluble in both solvents was considered as a mixture of GEOC and GEOC grafted PA11. The analysis of the data presented in Figure 5 indicated that with increasing GEOC content in the blend the amount of grafted PA11 increased, suggesting the increase of PA11 phase melt viscosity and confirming the reaction between GEOC and PA11.

3.2 Morphology

The combination of PPO and PA11 could lead to high performance blends because of their complementary properties. However, PPO and PA11 are incompatible and the properties of the blend are largely determined by their morphology [12, 13, 26]. Figure 6 shows SEM images of the fractured surfaces of PPO/PA11 (20/80) blends with various content of rubber-type compatibilizer (GEOC). It is necessary to point out that PPO is a matrix phase, though it is a minority composition of the blends [5]. This indicates that PPO formed the continuous phase (dark gray background), and PA11 and GEOC the dispersed phase (white and light gray particles). In fact, PPO had much higher melt viscosity than PA11, and tended to coalesce during melt blending [1]. Then a typical droplet-matrix morphology was obtained for PPO/PA11 (20/80) blend, where the dispersed spherical PA11 particles (mostly larger than 1 μm) with different dimensions could be easily identified, indicating macrophase separation. As could be expected, the addition of 15 wt% EOC remarkably increased the size of the dispersed particles. The large number of holes left by the dispersed particles when the sample was broken observed for the blend without GEOC as well as for the one with EOC, suggests poor adhesion between the phases. On the contrary, the particles' size significantly decreased with increasing amount of GEOC, and the fractured surfaces exhibited larger deformation when compared to the blend without GEOC as well as the one with EOC, which was attributed to the improved compatibility.

To further investigate the dispersion of GEOC in PPO/PA11 (20/80) blend, the fractured surfaces were observed with SEM after being etched either by nitric acid or chloroform to obtain a clear image of each phase, as shown in Figure 7. Nitric acid and chloroform are good solvents for PA11 and PPO, respectively, but non-solvents for GEOC. The SEM micrographs of PPO phase are provided in Figure 7a–e, while Figure 7f presents an SEM image of PA11 phase. The SEM micrographs of PPO/PA11 (20/80) blend are presented in Figure 7a,b, where the black holes indicate the PA11 phase etched by nitric acid, as marked by arrows in the images, which confirms that PPO formed the continuous phase, which is consistent with the reported results [5]. It is clear from Figure 7a,b that PA11 domains have a large size of about 2 μm , while much larger PA11 domains (about 3 μm) were observed in the presence of EOC (Fig. 7b). From Figure 7c,d, a uniform dispersion of the holes corresponding to the extracted PA11 domains can be observed, most of them being less than 0.2 μm . Moreover, the white domains corresponding to the GEOC can be seen. The GEOC was rather well dispersed with the presence

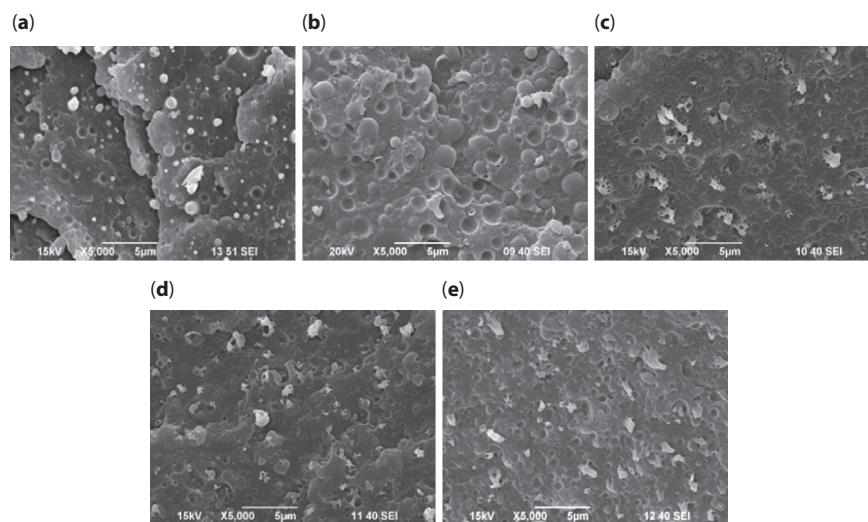


Figure 6 SEM micrographs of PPO/PA11 (20/80) blends: (a) without GEOC, (b) 15 wt% EOC, (c) 5 wt% GEOC, (d) 10 wt% GEOC, (e) 15 wt% GEOC.

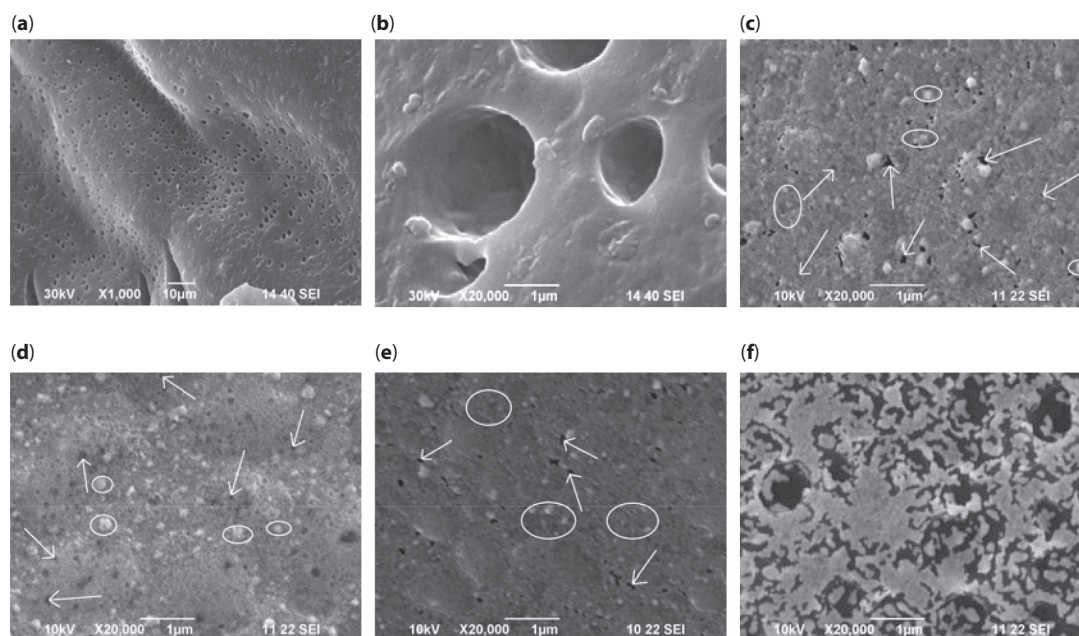


Figure 7 SEM micrographs of PPO/PA11 (20/80) blends etched by nitric acid: (a,b) without GEOC, (c) 5 wt% GEOC, (d) 10 wt% GEOC, (e) 15 wt% GEOC and (f) 15 wt% GEOC etched by chloroform; circles – GEOC, arrows – PA11 phase.

of a few small aggregates, as marked by circles in the images. It is evident that GEOC played a key role in reducing the domain size of PA11 in the PPO/PA11/GEOC/GEOC-PA11 blends. It might be attributed to the decrease of interfacial tension between PPO and PA11 in the case where the GEOC content was not very high, as PA11 domains are difficult to break up. With further increasing GEOC content, the blend morphology significantly changed from droplet-matrix to co-continuous structure (Figure 7e,f). This co-continuous

morphology was caused by the aggregation of GEOC segments and formation of GEOC-PA11 copolymers. A network of GEOC domain was considered to be more effective than the individual particles in stopping the growth of the cracks (see Table 2). This phenomenon could be explained by the influence of GEOC on the melt viscosity of the component polymers [1,8]. Moreover, it can be expected that GEOC is selectively located in the PA11 phase, which is due to the reaction of the epoxy group in the GEOC with the

amine end groups of PA11, as illustrated in Figure 1. The uniformly distributed GEOC in the PA11 phase increased the mobility of the PA11 chains, resulting in improved melt viscosity (lower MFR, see Table 3). When the melt viscosity of the PA11 phase was equivalent to that of PPO, the morphology of the blends transformed to co-continuous structure, in which both PA11 and PPO phases are continuous (see Figure 7e,f). It is clear from Figures 6 and 7 that the GMA grafts improved the compatibility as a result of chemical reactions with the amine group on PA11, which generated covalent bonds between the two polymers [8]. When the GEOC content in the PPO/PA11 blend was 15 wt%, the average size of GEOC particles was less than 0.1 μm , resulting in high toughness (see Table 3). Moreover, the size of the dispersed PA11 phase significantly decreased with increasing GEOC content. It can be concluded that when enough graft copolymers of GEOC-PA11 are generated *in situ*, they may act as a compatibilizer to lower the interfacial tension and stabilize the dispersed phases from coalescence [5, 8]. Hence, finer PA11 dispersed phase in the PPO matrix is formed. Finally, the droplet-matrix morphology is transformed to co-continuous structure.

Table 2 Effect of GEOC content on DSC data.

Sample	PPO phase	PA11 phase		
	T_g ($^{\circ}\text{C}$)	T_m ($^{\circ}\text{C}$)	T_c ($^{\circ}\text{C}$)	X_c (%)
PPO	215	–	–	–
PA11	–	188	156	16.6
PPO/PA11	215	187	159	12.1
15 wt.% EOC	215	187	159	11.8
5 wt.% GEOC	215	186	157	10.6
10 wt.% GEOC	215	186	157	9.3
15 wt.% GEOC	215	183; 186	160	9.7

3.3 Melting and Crystallization Behaviors

The compatibility of polymer blends can also be investigated by their melting and crystallization behaviors based on DSC measurements. The values of glass transition temperature (T_g), melting temperature (T_m), crystallization temperature (T_c) and degree of crystallinity (X_c) are reported in Table 2. The DSC thermograms of PA11 and various PPO/PA11 blends are presented in Figure 8. The analysis of DSC data indicated that the glass transition temperature (T_g) of the blends (corresponding to the neat PPO) was not affected by the presence of GEOC. The melting point (T_m) of PA11 shifted towards lower temperature with increasing GEOC content, due to the higher amount of *in situ* formed copolymers, as mentioned above; thus, to some extent interfered with the crystallization of PA11. As a result, the PA11 imperfect crystallites were formed, which resulted in the reduction of their melting temperature [5]. Moreover, PPO/PA11 (20/80) blend and PPO/PA11 containing 5–10 wt% GEOC showed a single melting peak, while the blend with 15 wt% GEOC exhibited double peaks. It is clear that the incorporation of 15 wt% GEOC resulted in the transformation of α -crystal form of PA11 to γ -crystal form, and also reflected changes in crystalline thickness and distribution of the α form [27, 28], which might be attributed to the restricted crystallization of PA11 particles in PPO/PA11. Therefore, the GEOC affected the crystallinity of PA11. Upon cooling (see Figure 8b), the peak temperature of melt crystallization of PA11 shifted to a lower temperature when 5–10 wt% of GEOC was added. However, the incorporation of 15 wt% GEOC increased T_c from 157 to 160 $^{\circ}\text{C}$, which was 4 $^{\circ}\text{C}$ higher compared to pure PA11, thus suggesting that GEOC might act as a nucleating agent to increase the crystallization rate of PA11. Moreover, PA11 crystallinity of the PPO/PA11/GEOC blends

Table 3 Mechanical properties and melt flow rate (MFR) of PPO, PA11 and various PPO/PA11 blends.

Samples	Notched Charpy impact strength (kJ/m^2)	Tensile modulus (MPa)	Tensile strength (MPa)	Elongation at break (%)	MFR ($\text{g}/10 \text{ min}$)
PPO	6 ± 1.2	2514 ± 49	70 ± 0.2	55 ± 1	4*
PA11	15 ± 1.6	1238 ± 65	47 ± 0.6	299 ± 9	22
PPO/PA11	9 ± 1.1	1291 ± 41	47 ± 0.9	245 ± 7	13
15 wt. % EOC	12 ± 2.0	1278 ± 54	34 ± 0.8	52 ± 11	24
5 wt. % GEOC	20 ± 1.7	1446 ± 69	43 ± 0.3	78 ± 1	9
10 wt. % GEOC	24 ± 2.0	1234 ± 56	38 ± 0.5	167 ± 5	8
15 wt. % GEOC	34 ± 1.8	1119 ± 76	38 ± 0.8	242 ± 3	5

*300 $^{\circ}\text{C}/5 \text{ kg}$

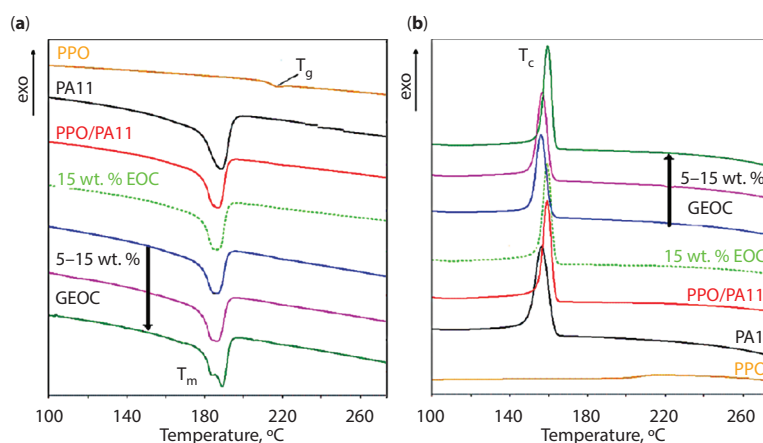


Figure 8 DSC second heating (a) and cooling (b) curves of PPO, PA11 and various PPO/PA11 blends.

decreased remarkably compared to that of pure PA11, uncompatibilized PPO/PA11 blend and the one with EOC, which confirmed that GEOC restricted the crystallization of PA11. The lower melting temperature and higher crystallization temperature of the PPO/PA11/GEOC blends compared to PA11 indicated that the reactions between the epoxy groups of GEOC with the amine groups of PA11 occurred successfully during the melt blending and GEOC-PA11 copolymers were formed (see Table 2).

3.4 Mechanical Properties and Dynamic Mechanical Properties

Tensile strength, impact strength and melt flow rate (MFR) of PPO, PA11 and various PPO/PA11 blends are listed in Table 3. The data indicates that GEOC had a major effect on the toughness. The notched Charpy impact strength of PPO/PA11/GEOC blends was much higher compared to PPO/PA11 blend as well as the one with EOC. The impact strength of PPO/PA11 blend was 9 kJ/m². It increased dramatically to 20 kJ/m² when 5 wt% GEOC was added, and further increased with the amount of functionalized EOC. Functional groups like GMA grafts can toughen PPO/PA11 blends in two ways. Firstly, the GMA graft imparts a higher polarity to the EOC, which then helps to improve the compatibility between PPO and PA11. As a result, GEOC is well dispersed and the particle size decreases, and thus a more efficient toughening is observed. Secondly, and more importantly, the GMA grafted onto EOC reacts with the amine end groups of PA11, which generates covalent bonds between the two polymers [8]. Therefore, the interfacial adhesion between PPO/PA11 blend and GEOC can be improved significantly. However, the addition of EOC also increased the impact strength of PPO/PA11 blend

(from 9 to 12 kJ/m²) thanks to the high content of rubber-type elastomer.

According to SEM results and the well-known toughening mechanism [29], GEOC particles are uniformly dispersed in the PA11 dispersed domains, which may induce the shear and craze yielding of the polymer phase, resulting in increased toughness. In other words, they activate the polymer layer surrounding them, and the motion of polymer segments consumes a major part of external energy, resulting in toughening. Wang *et al.* [12] reported that if the amount of maleic anhydride grafted elastomer particles was low, the thickness of the activated layer was much smaller than the average half distance between the particles, and moderate toughening could be observed. When the thickness of the activated layer approaches the average half distance between the particles, a brittle-ductile transition occurs.

PA11 is a relatively tough material, showing yielding behavior in the stress-strain curve (Figure 9). On the contrary, PPO is a brittle high-strength polymer. However, the addition of 20 wt% of PPO to the PA11 decreases elongation at break, and especially impact strength, which is much lower compared to PA11, maintaining yielding behavior of PA11 matrix.

Table 3 and Figure 9 illustrate the effect of GEOC content on tensile properties. Moreover, tensile properties of the blends were compared to the one with EOC. Despite the fact that the interfacial adhesion of EOC and PPO/PA11 matrix was improved by incorporating functional groups, the content of functionalized EOC increased, the tensile strength decreased and the elongation at break increased. This phenomenon can be explained by the fact that functionalized EOC is a flexible rubber-type polyolefin. Its presence in the blends would remarkably soften the material and increase the mobility of polymer chains, thus resulting in a slight decrease of tensile strength but a significant

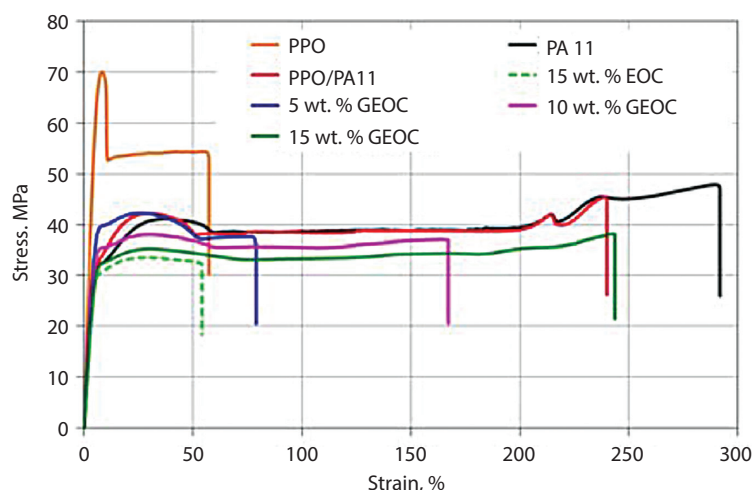


Figure 9 Stress-strain curves of PPO, PA11 and various PPO/PA11 blends.

Table 4 The results of DMTA analysis for PPO, PA11 and various PPO/PA11 blends.

Sample	Storage modulus (MPa)		Loss modulus peak position (°C)		
	at -50 °C	at 23 °C	T_{α}	T_{β}	T_{γ}
PPO	1150	1070	180	-16	-117
PA11	859	706	53	-69	-140
PPO/PA11	658	549	53	-71	-140
15 wt.% EOC	534	389	53	-54	-138
5 wt.% GEOC	657	520	52	-74	-141
10 wt.% GEOC	674	476	50	-74; -52	-141
15 wt.% GEOC	658	389	50	-70; -53	-142

increase of elongation at break. On the contrary, the blend in the presence of EOC showed a remarkable decrease of tensile strength (over 28%) and elongation at break (79%) as a result of poor adhesion at the interface, as was mentioned above. As expected, the tensile modulus decreased while the content of GEOC increased.

It is clear from Table 3 that the melt flow rate (MFR) of the blends decreased with the amount of GEOC. This indicates a higher degree of compatibilization [12, 21]. It can be explained by the reaction between GMA of the GEOC and the amine group of PA11, which increased molecular weight and the degree of branching, resulting in lower MFR (see Table 4). On the contrary, the addition of 15 wt% EOC resulted in significantly higher MFR, suggesting no chemical reactions between EOC and PA11.

The temperature dependence of the storage modulus G' of PPO, PA11 and various PPO/PA11 blends is shown in Figure 10a. Three distinct decreases were observed on the curves, corresponding to the chain segments relaxation of PA11 and PPO, respectively. It is clear that the addition of GEOC decreased the

G' of the blend in the whole test temperature range (see Table 4). It is particularly interesting to point out that in the temperature range from -150 to 23 °C the blends with GEOC showed higher storage modulus compared to the one with EOC. The addition of GEOC changed the phase structure of the blend, as shown in Figures 6 and 7. Such a change led to a sensitive response in the dynamic behavior. GMA grafts of EOC strongly interacted with the amine group of PA11, leading to a strong toughening effect of GEOC on PA11 chains. Consequently, PPO/PA11 containing 15 wt% GEOC had the lowest G' . However, for 5–10 wt% of GEOC, the interaction between the GEOC and PA11 was too weak, hence the decrement in G' is not significant. These results are in good agreement with tensile modulus, as shown in Table 3.

The temperature dependence of loss modulus (G'') for PPO, PA11 and various PPO/PA11 blends are shown in Figure 10b. The peaks on the curve correspond to α , β and γ relaxation of the polymers. The values of T_{α} , T_{β} and T_{γ} are presented in Table 4. The α , β and γ transitions of PPO were at 180, -16 and -117 °C, respectively. For the PPO/PA11 blend, a G'' peak at about 53 °C

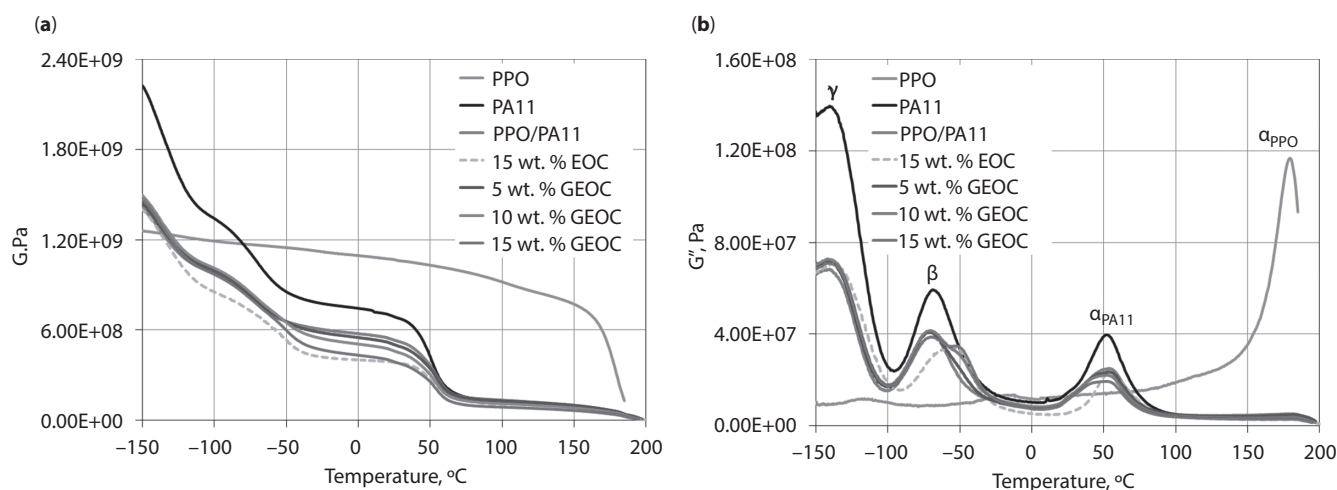


Figure 10 Storage modulus G' (a) and loss modulus G'' (b) as a function of temperature for PPO, PA11 and various PPO/PA11 blends.

corresponded to the glass transition temperature (T_g) of PA11, as shown in Figure 10b [30]. The T_g of PPO could not be detected since it was too close to the melting point of PA11 in the temperature range from 170 to 195 °C. With increasing GEOC content, the T_g peak of PA11 became much weaker and shifted to lower temperature, which could be attributed to the fact that the mobility of PA11 chain segments was largely restricted by the addition of GEOC. The analysis of the DMTA data also indicated that T_α of the PPO/PA11 blend was not affected by the presence of EOC.

The β relaxation was observed as a weak maximum in loss modulus for PPO. On the contrary, PA11, PPO/PA11 (20/80) blend and PPO/PA11 with 5 wt% GEOC had a clear single β relaxation peak centered at -69 , -71 and -74 °C, respectively. A single β relaxation peak was also observed for the blend with EOC. However, the value of T_β was significantly higher compared to PPO/PA11 blend. On the contrary, the second weak maximum of β relaxation appeared for the blend with 10 wt% GEOC content. This effect increased with increasing GEOC content, which is consistent with the DSC results. Moreover, with increasing GEOC content lower T_β shifted to the higher value, while the higher T_β to slightly lower. It was reported that the β relaxation results from motions of amide polar groups of polyamide in the interfacial region and is attributed to the glass transition [31]. The β relaxation temperature of the blends was 1–3 °C and 52–54 °C lower compared to PA11 and PPO, respectively.

The γ relaxation has been associated with a single relaxation process, predominantly of amorphous origin. The γ relaxation appeared as a maximum at -117 °C for PPO, which is 23 °C higher than that observed for

PA11 (Fig. 10b, Table 4), with a corresponding decrease in storage modulus (Fig. 10a). For the PPO/PA11, the γ relaxation was observed at -140 °C, which is 23 °C lower than that for PPO. No significant effect was observed by incorporating GEOC as well as EOC into PPO/PA11 on the γ relaxation. However, the blend with 10 wt% GEOC exhibited the lowest T_γ as a consequence of the lowest crystallinity (see Table 2).

4 CONCLUSIONS

Glycidyl methacrylate grafted ethylene-*n*-octene copolymer (GEOC) was used as an impact modifier for PPO/PA11 (20/80) blend, and reactive compatibilization was achieved via melt extrusion. The SEM results showed that PPO formed the continuous phase, though it is a minority component of the blends. With increasing GEOC content from 5 to 15 wt%, the morphology of PPO/PA11/GEOC blends changed from droplet-matrix to co-continuous morphology, which could be mainly attributed to the change in rheological behavior of the blend components as a result of the reaction between epoxy group of GEOC and amine end group of PA11. The co-continuous structure was more effective than individual particles in stopping the growth of cracks. The impact strength of PPO/PA11/GEOC blends achieved an optimum value of 34 kJ/m². PPO/PA11 containing 5 wt% GEOC exhibited a single T_m and T_β , while the blends with 10 and 15 wt% GEOC had double T_m and T_β . The addition of 15 wt% GEOC induced the transformation of α -crystal form of PA11 to γ -crystal form. It might be attributed to the restricted crystallization of PA11 particles in

PPO/PA11. The GEOC decreased the tensile modulus and storage modulus. Moreover, tensile strength decreased with GEOC content, whereas elongation and impact strength increased.

ACKNOWLEDGMENTS

This work was financially supported by project No. WND-POIG.01.03.01-14-058/09 co-financed by the European Union through the European Regional Development Fund. The authors are grateful to Dr. Aneta Łukomska and Maciej Studziński, M.Sc., of the Industrial Chemistry Research Institute, for providing the SEM microphotographs and DMTA analysis, respectively.

REFERENCES

1. B. Li, Y. Zhang, S. Wang, and J.L. Ji, Effect of POSS on morphology and properties of poly(2,6-dimethyl-1,4-phenylene oxide)/polyamide 6 blends. *Eur. Polym. J.* **45**, 2202–2210 (2009). DOI: 10.1016/j.eurpolymj.2009.04.010L
2. L. Arboleda-Clemente, A. Ares-Pernas, X. Garcia, S. Dopico, and M.J. Abad, Influence of polyamide ratio on the CNT dispersion in polyamide 66/6 blends by dilution of PA66 or PA6-MWCNT masterbatches. *Synth. Met.* **221**, 134–141 (2016). DOI: 10.1016/j.synthmet.2016.07.030
3. M. Sahnoune, A. Taguet, B. Otazaghine, and M. Kaci, Effects of functionalized halloysite on morphology and properties of polyamide-11/SEBS-g-MA blends. *Eur. Polym. J.* **90**, 418–430 (2017). DOI: 10.1016/j.eurpolymj.2017.03.008
4. Y. Li and G. Yang, An unusual morphology and crystallization behavior in situ formed polyphenylene oxide/polyamide 6 blends. *J. Mater. Sci.* **45**, 987–992 (2010). DOI: 10.1007/s10853-009-4029-z
5. Y. Ji, J. Ma, and B. Liang, In situ polymerization and in situ compatibilization of polymer blends of poly(2,6-dimethyl-1,4-phenylene oxide) and polyamide 6. *Mat. Lett.* **59**, 1997–2000 (2005). DOI: 10.1016/j.matlet.2005.02.021
6. J.J. Laverty, T. Ellis, J. Ogara, and S. Kim, Effect of processing on the recyclability of nylon 66/poly(2,6 dimethyl-1,4 phenylene oxide) (PPO) alloys. *Polym. Eng. Sci.* **36**, 347–357 (1996). DOI: 10.1002/pen.10421
7. Y. Li and H. Shimizu, Novel morphologies of poly(phenylene oxide) (PPO)/polyamide 6 (PA6) blend nanocomposites. *Polymer* **45**, 7381–7388 (2004). DOI: 10.1016/j.polymer.2004.09.018
8. D. Wu, X. Wang, and R. Jin, Toughening of poly(2,6-dimethyl-1,4-phenylene oxide)/nylon 6 alloys with functionalized elastomers via reactive compatibilization: Morphology, mechanical properties, and rheology. *Eur. Polym. J.* **40**, 1223–1232 (2004). DOI: 10.1016/j.eurpolymj.2004.01.004
9. X. Wang and H. Li, Compatibilizing effect of diglycidyl ether of bisphenol-A in polymer blend system: Nylon 6 combined with poly(butylacrylate) core and poly(methyl methacrylate) shell particles. *J. Appl. Polym. Sci.* **77**, 24–29 (2000). DOI: 10.1002/(SICI)1097-4628(20000705)77:1<24::AIDAPP4>3.0.CO;2-K
10. C.R. Chiang and F.C. Chang, Polymer blends of polyamide-6 (PA6) and poly(phenylene oxide) (PPO) compatibilized by styrene-maleic anhydride (SMA) copolymer. *Polymer* **38**, 4807–4817 (1997). DOI: 10.1016/S0032-3861(96)00015-8
11. R.R. Gallucci, Polyphenylene ether polyamide blends, US Patent 5260374, assigned to General Electric Co (09.11.1993).
12. X. Wang, W. Feng, H. Li, and R. Jin, Compatibilization and toughening of poly(2,6-dimethyl-1,4-phenylene oxide)/polyamide 6 alloy with poly(ethylene-1-octene): Mechanical properties, morphology, and rheology. *J. Appl. Polym. Sci.* **88**, 3110–3116 (2003). DOI: 10.1002/app.11987
13. Y. Son and S. Lee, One step method for fabrication of PPO/PA-66/elastomer blends. *Polymer Bulletin* **56**, 267–273 (2006). DOI: 10.1007/s00289-005-0473-3
14. Y.C. Lai, Graft copolymers of nylon 6 and polyphenylene oxide: Syntheses and their role in compatibilizing nylon 6/polyphenylene oxide blends. *J. Appl. Polym. Sci.* **54**, 1289–1296 (1994). DOI: 10.1002/app.1994.070540910
15. L. Martino, L. Basilissi, H. Farina, M.A. Ortenzi, E. Zini, G. Di Silvestro, and M. Scandola, Bio-based polyamide 11: Synthesis, rheology and solid-state properties of star structures. *Eur. Polym. J.* **59**, 69–77 (2014). DOI: 10.1016/j.eurpolymj.2014.07.012
16. A. Bourmaud, A. Le Duigou, C. Gourier, and C. Baley, Influence of processing temperature on mechanical performance of unidirectional polyamide 11-flax fibre composites. *Ind. Crops Prod.* **84**, 151–165 (2016). DOI: 10.1016/j.indcrop.2016.02.007
17. A. Le Duigou, A. Bourmaud, C. Gourier, and C. Baley, Multi-scale shear properties of flax fibre reinforced polyamide 11 biocomposites. *Composites Part A* **85**, 123–129 (2016). DOI: 10.1016/j.compositesa.2016.03
18. L. Yang and J.L. Thomason, Interface strength in glass fibre-polypropylene measured using the fibre pull-out and microbond methods. *Compos. Part A: Appl. Sci. Manuf.* **41**, 1077–1083 (2010). DOI: 10.1016/j.compositesa.2009.10.005
19. C. Gourier, A. Bourmaud, A. Le Duigou, and C. Baley, Influence of PA11 and PP thermoplastic polymers on recycling stability of unidirectional flax fibre reinforced biocomposites. *Polym. Degrad. Stab.* **136**, 1–9 (2017). DOI: 10.1016/j.polymdegradstab.2016.12.003
20. R. Jeziorska, B. Swierz-Motysia, M. Zielecka, A. Szadkowska, and M. Studzinski, Structure and mechanical properties of low-density polyethylene/spherical silica nanocomposites prepared by melt mixing: The joint action of silica's size, functionality, and compatibilizer. *J. Appl. Polym. Sci.* **125**, 4326–4337 (2012). DOI: 10.1002/app.36579
21. R. Jeziorska, B. Swierz-Motysia, A. Szadkowska, M. Studzinski, J. Dzierzawski, J. Kolasa, and I. Leszczynska, Method of production of impact modifiers for engineering polymers, Polish Patent 211 107 (April 30, 2012).

22. R. Jeziorska, B. Świerz-Motysia, and A. Szadkowska, Modifiers applied in polymer recycling: Processing, properties and application. *Polimery* **55**, 748–756 (2010).
23. R. Jeziorska, Z. Wielgosz, A. Abramowicz, A. Szadkowska, M. Zielecka, J. Dzierzawski, R. Komornicki, T. Jaczewska, and S. Firlik, High-impact thermoplastic compositions containing poly(phenylene oxide), Polish Patent 224 607 (January 31, 2017).
24. P. Ricou, E. Pinel, and N. Juhasz, Temperature experiments for improved accuracy in the calculation of polyamide-11 crystallinity by X-ray diffraction. *Adv. Xray Anal. Int. Cent. Diffraction Data* **48**, 170–175 (2005).
25. K.M. Sinotta, Mechanical relaxations in single crystals of polyethylene. *J. App. Phys.* **37**, 3385–3399 (1966). DOI: 10.1063/1.1708869
26. C. Harrats, S. Thomas, and G. Groeninckx, *Micro- and Nanostructured Multiphase Polymer Blend Systems*, CRC Press, Boca Raton (2006).
27. R. Jeziorska, B. Swierz-Motysia, A. Szadkowska, B. Marciniec, H. Maciejewski, M. Dutkiewicz, and I. Leszczynska, Effect of POSS on morphology, thermal and mechanical properties of polyamide 6. *Polimery* **56**, 809–816 (2011).
28. L.M. Liu, Z.N. Qi, and X.G. Zhu, Studies on nylon 6/clay nanocomposites by melt-intercalation process. *J. Appl. Polym. Sci.* **71**, 1133–1138 (1999). DOI: 10.1002/(SICI)1097-4628(19990214)71:7<1133::AID-APP11>3.0.CO;2-N
29. S. Wu, Phase structure and adhesion in polymer blends: A criterion for rubber toughening. *Polymer* **26**, 1855–1863 (1985). DOI: 10.1016/0032-3861(85)90015-1
30. K.P. Menard, *Dynamic Mechanical Analysis*, CRC Press, Florida (1999).
31. S.S. Ray and M. Okamoto, Polymer/layered silicate nanocomposites: A review from preparation to processing. *Prog. Polym. Sci.* **28**, 1539–1641 (2003). DOI: 10.1016/j.progpolymsci.2003.08.002